Frequency conversion in two-dimensional photonic structure

Babic, L.

Chapter 5

Interpretation of Fano lineshape reversal in the reflectivity spectra of photonic crystal slabs

5.1 Introduction

Asymmetric Fano lineshapes [66, 88] are a characteristic feature of (quantum) interference between two interfering paths and have been identified in many physical systems. These systems include, but are not limited to, neutron scattering [89], conductance of quantum dots [90,91], optical transmission through metal hole arrays [85, 92], scattering spectra of microwave cavities [93] and photonic crystal structures [58, 59, 94]. Recently, it has been suggested that the details of the Fano lineshape, in particular a complex valued q parameter, contains information on the decoherence and dephasing of the underlying quantum system [93, 95]. Similarly, reversal of the Fano lineshape asymmetry has been linked to the ability to tune the interaction, and thus also the coherence, between the two channels [90, 96].

Photonic crystal slabs, i.e., dielectric slabs perforated with a regular lattice of holes, show distinct Fano resonances in their reflection and transmission spectra. These photonic crystal slabs support optical modes for a combination of frequency ω and in-plane wave vector $k_{||}$, which are above the light line defined by $\omega = ck_{||}$, with c the speed of light in vacuum. These modes are either propagating (Fabry-Perot) modes of the slab, or leaky modes that couple incident light from the surrounding media to a guided mode of the slab via

This chapter is based on Lj. Babić and M. J. A. de Dood, *Interpretation of Fano lineshape reversal in the reflectivity spectra of photonic crystal slabs*, Opt. Express **18**, 26569–26582 (2010).

diffraction, picking up an additional crystal momentum equal to a reciprocal lattice vector. The interference of this resonant mode with the propagating Fabry-Perot mode leads to Fano resonances [57]. Typically, these resonant features in reflection spectra are used to find the dispersion relation of the leaky modes [58, 59, 94].

In most experimental studies the asymmetry parameter of the dispersive lineshape is considered to be constant and is regarded as a fit parameter. This asymmetry parameter, often denoted as q, can be interpreted as the amplitude of the resonant contribution relative to the background. The sign of q controls the asymmetry of the lineshape [66, 97]. In this picture, the asymmetry can only be reversed when the direct reflectivity reaches zero for which the lineshape becomes Lorentzian. The interference leading to the Fano lineshape in the reflectivity spectra of photonic crystal slabs can be tuned either via tuning the parameters of the structure, or via tuning the angle of incidence. Calculations at normal incidence for symmetric photonic crystal structures [98] confirm that this situation can be realized by tuning the ratio d/a of slab thickness over lattice constant. This shifts the resonance frequency of a leaky mode over a zero in the direct reflection of the slab and reverses the asymmetry. Experimentally this reversal has recently been demonstrated in reflection spectra of p-polarized light from a photonic crystal waveguide via angle tuning [67,99]. When the angle of incidence is tuned through Brewster's angle, the amplitude of the direct reflection reaches zero and the asymmetry is reversed. The symmetry of the system ensures that the reflectivity reaches a true zero and the amplitude reflection coefficient for the electric field changes sign, corresponding to a π phase shift. It is this phase shift that is responsible for the reversal of the asymmetry.

In this chapter we show that experimental reflectivity spectra for an asymmetric slab structure also show Fano lineshapes that reverse their asymmetry. This is surprising as these asymmetric structures generally do not give a true zero in the amplitude reflection coefficient; the interference leading to zeros in the reflectivity (Fabry-Perot modes) is not complete and the asymmetric structure does not have a Brewster's angle where the reflectivity for p-polarized light goes through zero. In order to describe the reversal of the asymmetry a complex q parameter is needed in a system that obeys both time reversal symmetry and energy conservation. We stress that the origin of the complex q in our work is not due to dephasing or decoherence as reported in literature [93, 95], but due to the asymmetry of the system. While dephasing and decoherence always result in a complex q parameter, the inverse statement is not true.

5.2 Experiment

Photonic crystal slabs with a square lattice of holes with a hole radius of ~ 150 nm and a lattice constant $a = 820$ nm were fabricated in a commercially grown AlGaAs layer structure [51] using a combination of e-beam lithography and reactive ion etching techniques. The samples were fabricated using the facilities of the Kavli Nanolab Delft. The layers of the AlGaAs layer structure are deposited on a $\langle 100 \rangle$ GaAs substrate and consist of a 1 μm thick Al rich $Al_{0.7}Ga_{0.3}As$ layer, a 150 nm thick Ga rich $Al_{0.35}Ga_{0.65}As$ layer, and a 100 nm thick GaAs capping layer. To create the hole pattern, a 150 nm silicon nitride layer is deposited on top of the structure and serves as a mask during the final reactive ion etching step. The lattice of holes is created by e-beam lithography in a ~ 500 nm thick layer of positive tone e-beam resist, ZEP 520A [52], and transferred into the nitride mask layer using a low pressure reactive ion etching step in a CHF_3/Ar plasma. After removal of the e-beam resist in a low pressure O_2 plasma, the hole pattern is etched deep into the AlGaAs heterostructure in a $BCl_2/Cl_2/N_2$ reactive ion etch process at 100 W RF power, a pressure of ~ 4.5 μbar, and flow rates of 15, 7.5, and 10 sccm respectively. The nitrogen flow in this process was optimized to create near vertical side walls of the holes. After etching the holes, the nitride mask is removed using the CHF_3/Ar etching procedure described above.

To create a freestanding membrane the residual oxide layer is first removed by dipping the sample in 15:1 deionized H_2O:buffered hydrofluoric acid (BHF) solution for 15 sec. The sample is then placed in a 3:1 citric acid:H_2O_2 solution for 120 sec to selectively remove the GaAs capping layer. The freestanding membrane is created by etching the sacrificial $Al_{0.7}Ga_{0.3}As$ layer in a concentrated 1:4 HF (40%):H_2O solution for 60 sec followed by a rinsing step in pure water and critical point drying. The resulting freestanding membrane covers an area of $\sim 300 \times 300$ μm^2 and is used to measure specular reflectivity spectra at oblique angles of incidence. Afterwards, the membrane is transferred to a transparent gel layer [80], with a refractive index of 1.4 on a standard microscope slide to create a membrane without the highly reflective GaAs substrate and the reflectivity measurement is repeated.

The specular reflectivity measurements are done for wavelengths between 900 and 1700 nm using white light from a lamp coupled to a 50 μm multimode fiber. The output of this fiber is imaged onto the sample with a 1.5 times magnification to create a 75 μm spot on the sample. The reflected light is collected into a 400 μm fiber and then sent to a fiber-coupled grating spectrometer with an InGaAs array (Ocean Optics NIR512) with a ≈ 3 nm spectral resolution. Apertures in the beam limit the numerical aperture of the

input beam to NA ~ 0.025. A Glan-Thompson polarizing beamsplitter cube is placed in a parallel part of the beam and is used to measure both the s- and p-polarized reflectivity as a function of wavelength and angle of incidence.

5.3 Results

The experimentally measured reflection spectra for the symmetric slab structure are shown in Fig. 5.1. The figure shows the measurements (symbols) and calculations based on a complete scattering matrix method (solid gray lines), for angles of incidence of 60° (left), 70° (middle), and 80° (right). The frequency ω and the wave vector $k_{||}$ are plotted in dimensionless units $\omega a/(2\pi c)$ and $k_{||}a/(2\pi)$, respectively. The incident beam is p-polarized with the parallel wave vector $\mathbf{k}_{||}$ oriented along the ΓX symmetry direction of the photonic lattice. The numerical calculations assume an ideal two-dimensional photonic crystal slab with air on both sides. The calculations use the tabulated

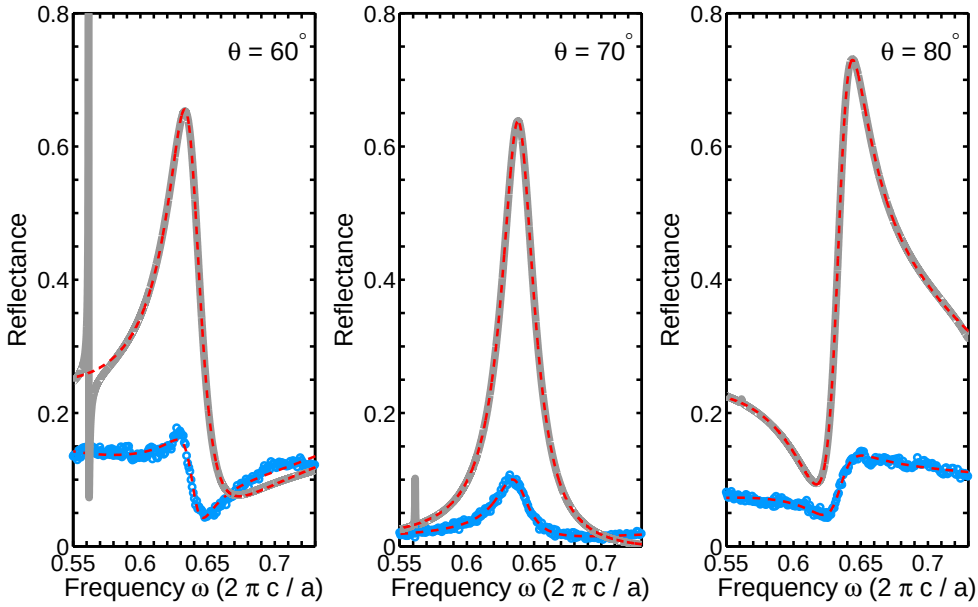

Figure 5.1. Measured (blue symbols) and calculated (solid gray lines) reflection spectra for different angles of incidence for a symmetric (freestanding) slab, showing the asymmetry reversal of the p-polarized (-1,±1) mode at Brewster's angle. The dashed red lines are fits to the data using the Fano model described in the text.

value for the refractive index of the $Al_{0.35}Ga_{0.65}As$ at a wavelength of 1.5 μm; $n_2 = 3.1975$ [62]. The thickness of the slab and the value of r/a are identical to those of the experimental structure. The calculations are performed for a structure with a lattice constant $a = 820$ nm, a radius of holes $r = 160$ nm, and a thickness of the slab $d = 122$ nm.

As can be seen in the figure, the calculations give good qualitative agreement with the data. Both the measured and the calculated reflectivity spectra are well described by the Fano lineshape. The dashed red lines in Fig. 5.1 show a fit using a Fano model, with the reflectivity $R(\omega)$ given by

$$R(\omega) = \left| r_D \exp(-i\Delta\xi) + \frac{r_R \Gamma_0}{i(\omega - \omega_0) + \Gamma_0} \right|^2 . \tag{5.1}$$

The first term represents the direct contribution with an amplitude r_D, while the second term represents the resonant contribution with an amplitude r_R. The resonance is characterized by a frequency ω_0, and a linewidth Γ_0. The phase $\Delta\xi$ represents the phase difference between the resonant and the non-resonant contribution at the resonance frequency and controls the asymmetry of the resonance. We assume that the amplitude of the slowly varying non-resonant contribution as a function of frequency ω, $r_D(\omega)$, can be approximated well with

$$r_D(\omega) = \left| r_0 + r_1\omega + r_2\omega^2 \right| , \tag{5.2}$$

where r_0, r_1 and r_2 are fit parameters.

The asymmetry of the Fano lineshape in Fig. 5.1 of the p-polarized (-1,$\pm$1) mode is reversed by tuning the angle of incidence, creating a nearly symmetric lineshape at an angle of incidence of 70°. Based on the asymmetry of the lineshape in reflectivity measurements for every 5° (not shown) we estimate that the asymmetry reversal occurs at an angle of incidence of $71 \pm 1°$. This corresponds to a Brewster's angle θ_B for a uniform dielectric slab in air with an effective refractive index of $\tan(\theta_B)$ equal to $n_{\text{eff}} = 2.9 \pm 0.2$. We expect this value to be comparable to the effective refractive index estimated from the direct (non-resonant) reflectivity of the slab at the resonance frequency. This contribution is modeled by the Fresnel reflection coefficients of the dielectric slab with an effective refractive index that represents the average effect of the holes. Since this background is close to zero for all frequencies for angles of incidence close to Brewster's angle we analyze calculated spectra over a broad frequency range for angles of incidence of 60° and 80°. From these fits, we obtain values of the effective refractive index of 3.02 and 2.89, consistent with the effective refractive index found from analyzing the asymmetry of the resonant contribution.

Table 5.1 summarizes the resonance frequency, the linewidth and the phase difference, as obtained from the Fano model for both the measured and calculated reflection spectra in Fig. 5.1. The table shows the excellent agreement between the measured and calculated spectra for the resonance frequency (ω_0) and the corresponding linewidth (Γ_0). The phase difference $\Delta\xi$ changes sign as the resonant Fano lineshape changes the asymmetry. The relatively large error bars for $\Delta\xi$ are representative for the variation in the fitted value of $\Delta\xi$ for different choices of the background (direct) contribution; e.g., by setting both r_1 and r_2 equal to zero in Eq. 5.2. Close to Brewster's angle for the symmetric slab, the background (direct) contribution reaches zero amplitude and the phase difference $\Delta\xi$ becomes undefined. The comparison between the experimental and calculated spectra presented above confirms the picture that the asymmetry reversal occurs around the true zero in the direct reflectivity at Brewster's angle.

After reflection measurements, the symmetric, freestanding, photonic crystal membrane was transferred to a transparent gel substrate by sticking the membrane to the gel and peeling of the GaAs substrate, as described in Chapter 4 of this thesis. The gel is optically transparent and has a refractive index $n_{gel} = 1.4$. Figure 5.2 shows measured (symbols) and calculated (solid gray lines) reflection spectra for an asymmetric slab for angles of incidence of 75° (left), 78° (middle), and 83° (right).

The experimental data in the figure clearly show that the asymmetry reversal of the Fano lineshape of the *p*-polarized (-1,±1) mode also occurs in the asymmetric case when there is no Brewster's angle. In this case, the asymmetry reversal is observed at a significantly larger angle of incidence of $78 \pm 1°$, compared to the symmetric structure. The parameters of the fitted Fano lineshapes are summarized in Table 5.1.

5.4 Discussion

A detailed inspection of the calculated spectra for the asymmetric structure (not shown) reveals that the amplitude of the direct reflectivity is low, but does not reach zero. This implies that a simple change of the sign of the amplitude reflection coefficient in the direct channel cannot be responsible for the reversal of the Fano lineshape. In order to convincingly show that a true zero in the direct reflectivity is not a necessary condition for the asymmetry reversal of a Fano lineshape we performed additional calculations on a structure with a much larger lattice constant. The parameters of this structure are tuned to give a minimum in the direct reflectivity that is very different from zero.

Table 5.1. Fitted values of the Fano resonances: the center frequency, the linewidth, and the phase difference between the resonant and the direct contribution in the reflectivity. Results are given for both measured and calculated spectra, for various angles of incidence for a symmetric slab (top) and an asymmetric slab on a substrate (bottom).

	angle (°)	ω_0 $(2\pi c/a)$	Γ_0 $(2\pi c/a)$	$\Delta\xi$ (rad)
Symmetric				
	60	0.640 ± 0.005	0.009 ± 0.001	−2.19 ± 0.10
Experiment	70	0.636 ± 0.005	0.015 ± 0.002	−0.58 ± 0.15
	80	0.635 ± 0.005	0.015 ± 0.002	1.90 ± 0.08
	60	0.639 ± 0.001	0.014 ± 0.001	−1.28 ± 0.02
Calculation	70	0.638 ± 0.001	0.014 ± 0.001	—
	80	0.635 ± 0.001	0.012 ± 0.001	1.68 ± 0.07
Asymmetric				
	75	0.611 ± 0.005	0.009 ± 0.001	−0.60 ± 0.06
Experiment	78	0.611 ± 0.005	0.009 ± 0.001	−0.13 ± 0.15
	83	0.610 ± 0.005	0.008 ± 0.001	0.51 ± 0.24
	75	0.620 ± 0.001	0.014 ± 0.001	−0.72 ± 0.24
Calculation	78	0.620 ± 0.001	0.014 ± 0.001	−0.06 ± 0.37
	83	0.618 ± 0.001	0.015 ± 0.001	1.26 ± 0.05

The calculations are performed for both a symmetric (air-slab-air) and an asymmetric (air-slab-gel) structure and are summarized in section 5.4.3.

The remainder of this chapter is structured as follows: we will first introduce a general scattering matrix formalism for asymmetric structures and apply this to the specific case of a photonic crystal slab on a substrate with only two inputs and two outputs. This results in analytical expressions for the reflected amplitude and the asymmetry parameter q of the Fano resonance. We then apply this truncated scattering matrix method to interpret our experimental data and compare the results to those obtained using a complete scattering matrix.

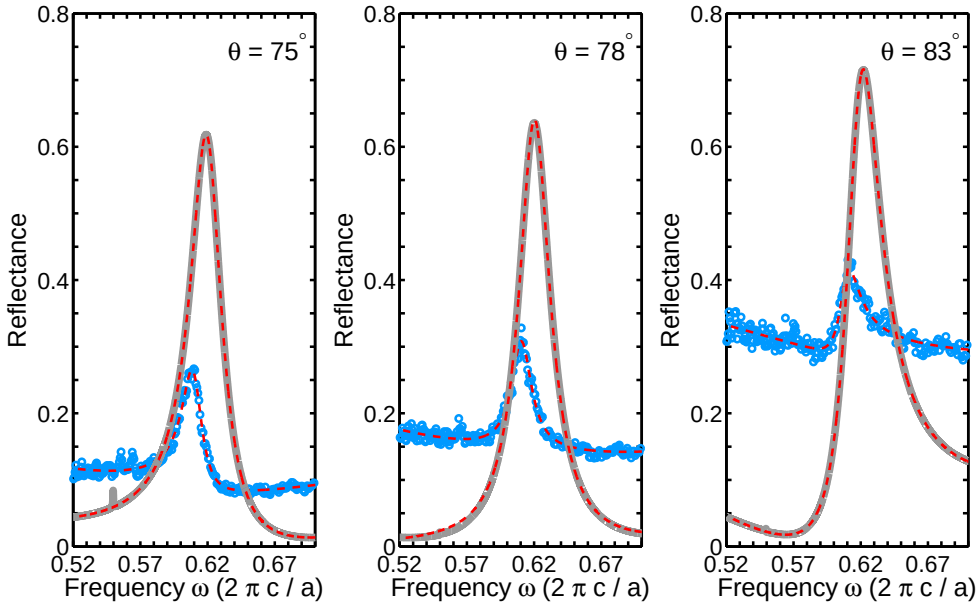

Figure 5.2. Measured (blue symbols) and calculated (solid gray lines) reflection spectra for different angles of incidence for an asymmetric (on gel) slab, showing the asymmetry flip of the *p*-polarized (-1,±1) mode. The dashed red lines are fits to the data using the Fano model described in the text.

5.4.1 Scattering matrix formalism

We introduce a scattering matrix formalism to describe the resonant coupling of incident radiation to a planar photonic crystal slab. Compared to earlier work [60], which deals with symmetric structures, our formalism deals with both symmetric and asymmetric photonic crystal waveguide structures. We will apply this formalism to the particular case of a planar photonic crystal slab on a substrate to gain physical insight in the origin of the asymmetry reversal of the dispersive (Fano) lineshape. We will give results for oblique angles of incidence for both symmetric (air-slab-air) and asymmetric (air-slab-gel) structures, and discuss the conditions for asymmetry reversal of the dispersive (Fano) lineshape in detail.

We consider an optical system with m inputs and m outputs that can be described by temporal coupled-mode theory featuring a $m \times m$ scattering matrix [60]. For the specific case of a photonic crystal slab the inputs and outputs of the system are defined by a plane wave incident on the slab that

is either transmitted, reflected or diffracted. The plane waves can couple to a guided mode in the photonic crystal membrane, thereby transforming the guided modes into leaky modes. This occurs whenever a photonic band in the band structure of a photonic crystal slab is above the light line. The resulting transmission and reflection spectra of a photonic crystal membrane contains several peaks, each with a dispersive (Fano) lineshape characteristic for the resonant coupling [58, 59, 94].

The input of the optical system is described by a column vector $\mathbf{b}_+$ that contains the amplitudes of the modes at the input. A similar vector $\mathbf{b}_-$ contains the amplitudes of the modes at the output. For a planar multilayer structure the amplitudes b_i in a medium with refractive index n_i are related to the E-field in the i-th layer by [100]

$$b_{\pm,i} = \sqrt{\frac{1}{2}\frac{k_{iz}}{k_0}} E_{\pm,i}, \tag{5.3}$$

where $k_0 = 2\pi/\lambda$ is the wave number and k_{iz} is the component of the wave vector perpendicular to the interface: $k_{iz} = n_i \cos\theta_i k_0$. To avoid confusion with the **E**-field, we will refer to these amplitudes as **b**-field amplitudes. This **b**-field amplitude is normalized in such a way that the square of the amplitude relates directly to the power flux, defined by the Poynting vector, in the z-direction normal to the interface. The scattering matrix S relates the amplitudes of input and output modes via

$$\mathbf{b}_- = S\mathbf{b}_+.$$

For a lossless system that does not break time-reversal symmetry the scattering matrix S needs to be unitary and symmetric [60]:

$$SS^\dagger = I, \quad S_{ij} = S_{ji}.$$

To describe the coupling to leaky modes we will characterize each mode at a specific in-plane wave vector $k_\parallel$ by a center frequency ω_p and a linewidth Γ_p. The linewidth Γ_p is related to the coupling strength between the incoming light and the leaky mode. The total scattering matrix of a layered structure with N independent resonances can be written as

$$S = C + \sum_{p=1}^{N} \frac{\mathbf{d_p} \otimes \mathbf{d_p}}{i(\omega - \omega_p) + \Gamma_p}. \tag{5.4}$$

Here $\mathbf{d_p}$ is a vector containing the coupling constants of each mode to the resonator, ω_p are the resonance frequencies, Γ_p denotes the resonance linewidth,

and C is a unitary and symmetric scattering matrix. Linear optical structures impose both time-reversal symmetry and energy conservation constraints on the system and require that the matrix elements of C, Γ_p, and the coupling constants $\mathbf{d_p}$ are not independent [60].

5.4.2 Example: 2-port asymmetric slab

For a system with 2 inputs and 2 outputs the relation between C, Γ, and $\mathbf{d}$ can be made explicit and insight can be gained by studying this case in more detail. Therefore, we will restrict ourselves to the simplest asymmetric photonic crystal structures where no higher order diffraction occurs. In that case the system has only two inputs and two outputs and the scattering matrix reduces to a 2×2 matrix. The inputs and outputs of this system correspond to the reflected and transmitted modes. Compared to the earlier work reported in Ref. [60] we do retain the essential asymmetry induced by the substrate. The photonic crystal slab has an effective refractive index equal to n_2 and is sandwiched between a substrate with a refractive index n_3 and a superstrate with a refractive index n_1.

The expressions for the asymmetric structure are identical to those of the symmetric structure if we refer to the amplitude reflection and transmission coefficients r' and t' of the **b**-field as defined by Eq. 5.3. The complete scattering matrix is given by

$$S = \begin{pmatrix} r' & t' \\ t' & r' \end{pmatrix} + \frac{\Gamma_0}{i(\omega-\omega_0)+\Gamma_0} \begin{pmatrix} -(r'\pm t') & \mp(r'\pm t') \\ \mp(r'\pm t') & -(r'\pm t') \end{pmatrix}, \tag{5.5}$$

where the $\pm$ sign corresponds to a situation where the E-field on both sides of the slab oscillates in phase or out of phase. For a symmetric slab this defines the modes as either *even* or *odd* relative to the symmetry plane in the middle of the slab [63]. The coefficients r' and t' are related to the more commonly used Fresnel coefficients r and t of the slab via $r' = r$ and $t' = t\sqrt{k_{3z}/k_{1z}}$ for both s- and p-polarized light [100].

The reflected intensity of the slab given by $R(\omega) = |S_{11}(\omega)|^2$ can be written in a form that is identical to the original result of Fano [66]:

$$R(\epsilon) = |S_{11}(\epsilon)|^2 = |r'|^2 \frac{|q+\epsilon|^2}{1+\epsilon^2}. \tag{5.6}$$

Here ϵ is the normalized detuning in units of the linewidth $\epsilon = (\omega-\omega_0)/\Gamma_0$,

and the asymmetry parameter q is given by

$$q = \pm i \, \frac{t'}{r'}. \tag{5.7}$$

A similar expression can be derived for the transmission with an asymmetry parameter $\tilde{q} = -q^{-1}$. For a symmetric slab q reduces to a real-valued parameter since the Fresnel transmission coefficient has a π phase difference with the reflection coefficient. This is no longer true for the more general case of an asymmetric slab for which the phase difference between t' and r' varies as a function of angle of incidence and the resulting q parameter is complex.

Figure 5.3 shows the calculated phase difference between the direct and the resonant contribution in the reflection of p-polarized light for the fundamental TE mode supported by a waveguide layer with an effective refractive index n_{eff} equal to 3.16 representative of the AlGaAs material used in the experiment.

For this calculation we used the matrix element S_{11} in Eq. 5.5 at the resonance frequency and we used complex Fresnel coefficients r and t defined as

$$r = \frac{r_{12} + r_{23} \exp[i2k_{2z}d]}{1 - r_{21}r_{23} \exp[i2k_{2z}d]} \exp[-i2k_{1z}d]$$

$$t = \frac{t_{23}t_{12} \exp[i(2k_{2z} - k_{1z} - k_{3z})d/2]}{1 - r_{21}r_{23} \exp[i2k_{2z}d]}.$$

Here the coefficients r_{ij} and t_{ij} refer to the Fresnel coefficients of a single interface between layer i and j. The figure shows the phase difference as a function of angle of incidence and dimensionless quantity $n_{\text{eff}}d/\lambda$. Figure 5.3 (a) shows the phase difference for a symmetric structure with air on both sides, while Fig. 5.3 (b) shows the phase difference for the same slab with the air on one side replaced by a transparent gel with refractive index $n_3 = 1.4$. This figure clearly shows large, abrupt jumps in the phase difference for both symmetric and asymmetric slab structures. The phase jumps in the symmetric case are easily understood as points where the direct reflectivity reaches zero. This occurs at Brewster's angle (vertical dashed line in (a)) and whenever the reflectivity becomes zero due to interference in the film (horizontal solid lines). This Fabry-Perot condition is satisfied whenever the optical path length of the film defined as $n_{\text{eff}}d\cos\theta$ is equal to $m\lambda/2$, with m integer. This situation changes for the asymmetric structure (b). The Fabry-Perot condition produces a minimum in the reflectivity, but the reflectivity does not reach zero. As can be seen in the figure, for angles smaller than $\arctan(n_3/n_1)$ the phase jumps at the minimum in the reflectivity. To understand the phase jump for larger

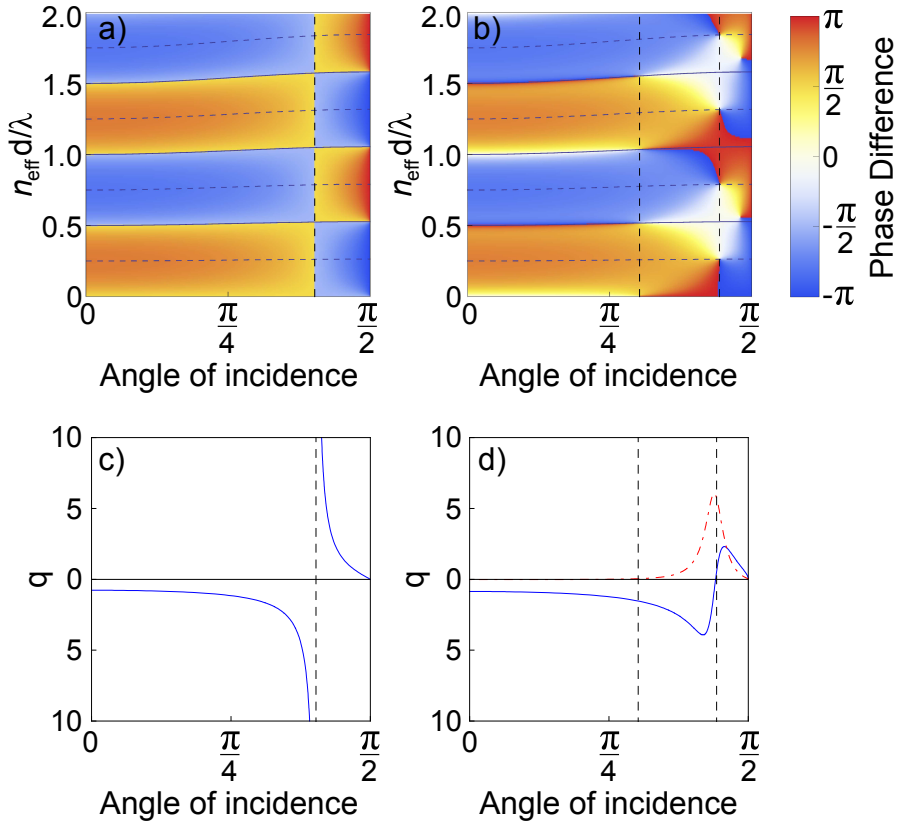

Figure 5.3. Calculated phase difference between the direct and the resonant contribution for a slab with an effective refractive index of 3.16, representative for AlGaAs used in the experiment. The plot shows the phase difference as a function of angle of incidence and dimensionless quantity $n_{\text{eff}}d/\lambda$ for a symmetric membrane structure (a) and an asymmetric structure on a gel substrate with $n_3 = 1.4$ (b). The solid and dashed lines are explained in the text. The corresponding asymmetry parameter q of the Fano resonance as a function of angle of incidence is shown for the symmetric (c) and asymmetric structure (d) for a value of $n_{eff}d/\lambda = 0.3$. The solid line refers to the real part of q, while the dash-dot line shows the imaginary part of q for the asymmetric structure.

angles of incidence we write the reflectivity of the asymmetric slab as [101]:

$$R = |r|^2 = \frac{{r_{12}}^2 + {r_{23}}^2 + 2r_{12}r_{23}\cos 2\beta}{1 + {r_{12}}^2{r_{23}}^2 + 2r_{12}r_{23}\cos 2\beta},$$

with $\beta = k_{2z}d$.

From this expression it is clear that the minima and maxima in the reflectivity are found by the condition

$$\cos 2\beta = \pm 1.$$

These conditions are indicated by the solid and dashed horizontal lines in the figure. The reflectivity of the asymmetric slab can only become zero for a specific combination of frequency and angle of incidence. The frequency at which the reflectivity becomes zero is given by the above condition, while the angle is defined by the additional condition that

$$r_{12} = \pm r_{23}.$$

This leads to two angles, indicated by the dashed vertical lines in Fig. 5.3 (b). The smallest of the two angles is independent of the refractive index of the layer n_2 and is equal to Brewster's angle $\arctan(n_3/n_1)$ between the superstrate and substrate [101]. The second angle depends on the refractive index of the slab, superstrate, and substrate material. For a slab with $d/a < 0.5$ this angle is always larger than Brewster's angle between the superstrate and the slab material. From the figure, it can be seen that the phase difference jumps for angles close to this larger angle for dimensionless quantities $n_{\text{eff}}d/\lambda$ that are not close to $m/2$, with m being integer. The value of the refractive index of the substrate plays an important role in determining the two angles and also controls the apparent repulsion between the phase jumps due to the Fabry-Perot effect and due to angle tuning.

The angle from the simple truncated scattering matrix model is consistent with the experimental results presented in Section 5.3. For a structure with an effective refractive index of 2.9 ± 0.2 on a substrate with a refractive index of 1.4, the minimum in the direct reflectivity (see the vertical dashed line in Fig. 5.3) occurs at an angle of $78.1 \pm 1.5°$. This number compares well with the experimental value of $78 \pm 1°$. Figures 5.3 (c) and (d) show the calculated asymmetry parameter q as a function of angle for a value of $n_{eff}d/\lambda = 0.3$. This value corresponds to the experimentally measured frequency of the Fano resonance of the symmetric structure at Brewster's angle. The real part of q is represented by the solid blue line, while the complex part of q is shown by

the red dash-dot line. For the symmetric structure the q is real-valued, while the q parameter for the asymmetric structure in Fig. 5.3 (d) is clearly complex with a non-trivial phase that depends on the angle of incidence.

5.4.3 Asymmetry reversal with nonzero background

In this section we present numerical data calculated by a complete scattering matrix method that show that the asymmetry of a Fano resonance can be reversed if the direct reflectivity does not reach zero. The parameters of the photonic crystal structure in the calculation are tuned to give a minimum in direct reflectivity that is very different from zero to more clearly illustrate the point. We consider a two-dimensional photonic crystal slab with a lattice constant $a = 2$ μm and use the same radius of holes $r = 160$ nm and slab thickness $d = 122$ nm as in the experimental structure. The refractive index of the slab material is taken to be $n_{slab} = 3.157$, equal to the infrared refractive index of $Al_{0.35}Ga_{0.65}As$ at a wavelength of 2.5 μm [62].

Figures 5.4 and 5.5 summarize the calculated reflection spectra and corresponding phase difference $\Delta\xi$ for the symmetric structure. These data should be compared to the data in Figures 5.6 and 5.7 obtained for the asymmetric structure.

The calculated reflection spectra in Figure 5.4 show the Fano lineshape reversal for the symmetric structure. Spectra are shown for angles of incidence from 68° to 76° in steps of 2° (solid lines) and are offset vertically by 0.8 for clarity. The horizontal dash-dot lines indicate the zero reflectance for each angle of incidence. The dashed lines show the fitted Fano lineshapes to data. As can be seen, the asymmetry of the Fano lineshape is reversed by tuning the angle of incidence. At Brewster's angle ($\theta = 72°$), the direct reflectivity reaches zero, and the Fano lineshape reduces to the symmetric Lorentzian lineshape of the resonant contribution.

The solid line in Fig. 5.5 shows the phase difference $\Delta\xi$ between the resonant and the non-resonant contribution, for the p-polarized (-1,$\pm$1) mode over a large range of angles. This phase difference is obtained at the resonance frequency, by fitting the Fano model of Eq. 5.1 to the calculated reflection spectra. The phase difference $\Delta\xi$ influences the interference between the direct and resonant reflectivity and controls the asymmetry of the Fano lineshape. Whenever this phase difference is an integer multiple of π radians, the asymmetry reversal of the Fano lineshape occurs. As can be seen in Figure 5.5, the phase difference goes through zero for an angle of incidence of 72°. This angle is exactly equal to Brewster's angle for the symmetric structure and the direct reflectivity is zero (see Fig. 5.4).

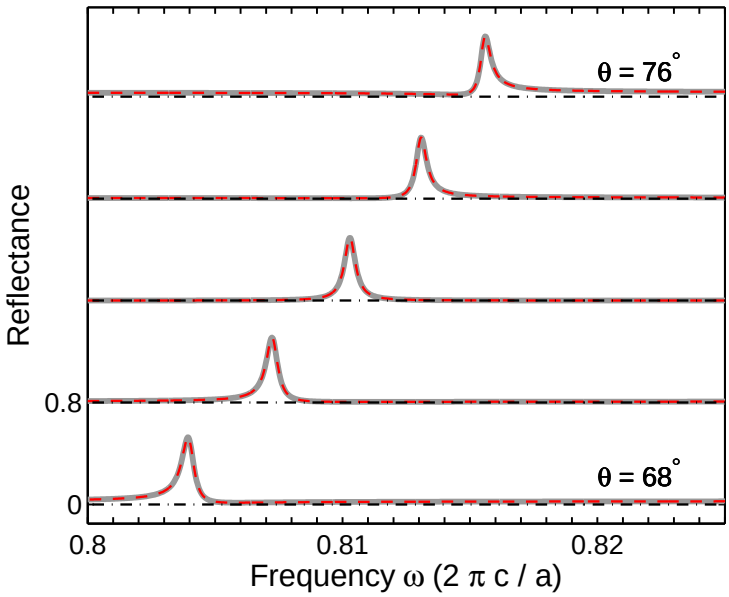

Figure 5.4. Calculated reflection spectra for a symmetric structure (solid lines), for angles of incidence from 68° to 76° in steps of 2°, vertically offset by 0.8 for clarity, showing the asymmetry reversal of the p-polarized (-1,±1) mode. The calculations are performed for a structure with a lattice constant $a = 2$ μm, a radius of holes $r = 160$ nm, and a slab thickness $d = 122$ nm. Note that the zero in the amplitude reflection coefficient is indicated by the dash-dot lines, for each reflectivity spectrum. The dashed lines show the fit of the Fano model to the calculated data.

Figure 5.5 shows a small, abrupt change, in the phase difference, for an angle of incidence of $\approx 12°$, as indicated by the vertical arrow. The origin of this phase change is an extra diffraction order of the leaky mode into the surrounding air. These diffraction orders occur whenever the length of the wave vector in air is larger or equal than the parallel component of the wave vector of the waveguide mode modulo a reciprocal lattice vector $\mathbf{G}$. In dimensionless units this diffraction condition is given by

$$|\mathbf{k_s}| = n_s\omega_0 > |\mathbf{k}_{||} + \mathbf{G}|, \tag{5.8}$$

where $\mathbf{k_s}$ is the wave vector in the substrate/superstrate and $\mathbf{k}_{||}$ is the parallel component of the incident wave vector, ω_0 is the dimensionless frequency of the resonance and n_s is the refractive index of the substrate/superstrate. The inset of Fig. 5.5 shows the dispersion $\omega_0(\theta)$ of the p-polarized (-1,±1) leaky

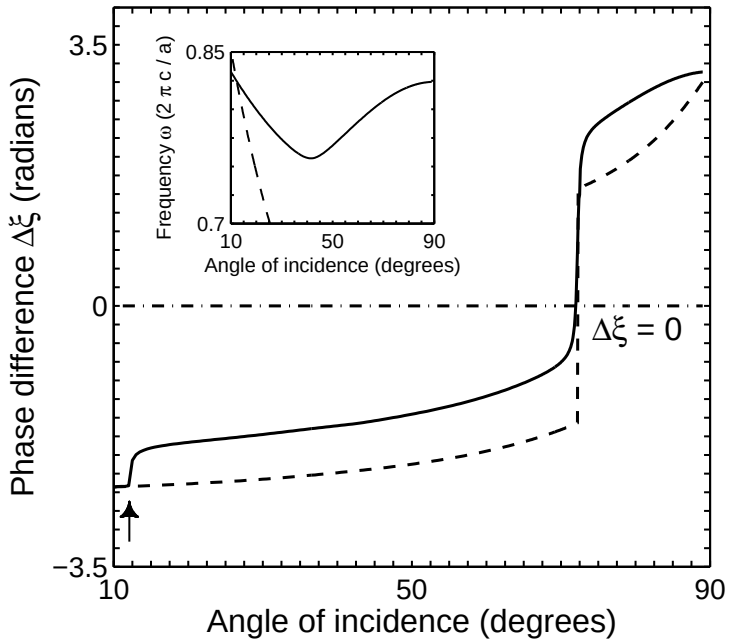

Figure 5.5. Calculated phase difference between the resonant and the non-resonant contribution, as a function of the angle of incidence, for a symmetric structure (solid line). The phase difference is obtained for the p-polarized (-1,±1) mode at the resonance frequency, by fitting a Fano model to the calculated reflection spectra. The asymmetry reversal of the Fano lineshape ($\Delta\xi = 0$) occurs at Brewster's angle. The dashed line represents the phase difference calculated using a coupled-mode theory with only two modes, as described in the text. The inset shows the calculated dispersion relation of the leaky mode (solid line), and the folded light line in air (dashed line).

mode (solid line) obtained from the calculated spectra together with the folded light line in air (dashed line)*. The crossing of these lines corresponds to the condition for diffraction in air, which occurs for angles larger than 12°.

How does the phase difference between the resonant and the non-resonant contribution compare to the phase difference calculated with the relatively simple coupled-mode theory of only two modes as presented in Section 5.4.2? To answer this question, we ignore the effect of higher diffraction orders and

*To convert in-plane wave vectors $k_{||}$ to angles of incidence θ for a mode with a dispersion $\omega(k_{||})$ in a medium with a refractive index n, we use the expression $\theta = \arcsin(k_{||}/(n\omega))$, with ω and $k_{||}$ expressed in dimensionless units $\omega a/(2\pi c)$ and $k_{||}a/(2\pi)$, respectively.

use the truncated 2×2 matrix to describe the system. The direct reflectivity of our slab can be well described by the reflectivity of a uniform slab with a frequency dependent effective refractive index n_2, which takes into account the extra dispersion due to the presence of the holes [57]. We fitted the Fano model to the calculated p-polarized reflection spectrum for an angle of incidence of 10°. For this angle there are no diffraction orders in air for the relevant (-1,±1) mode. The calculated reflection spectrum consists of sharp resonant features going from zero to unity superimposed on a slowly oscillatory background. The direct reflectivity is well described by an effective refractive index

$$n_2 = 3.118 - 0.014\omega + 0.029\omega^2, \tag{5.9}$$

with ω expressed in dimensionless units $\omega a/(2\pi c)$. Since the p-polarized (-1,±1) mode shows a flat dispersion (see inset of Fig. 5.5), the resonance frequency does not change significantly with $k_{||}$. Therefore, we assume that Equation 5.9 can be used for other angles of incidence as well. The dashed line in Fig. 5.5 shows the calculated phase difference using Eq. 5.5 and the known dispersion of the resonant mode. As can be seen, the agreement between the solid and the dashed line is excellent for angles below 12°. For angles larger than 12° there is a small deviation as the truncated two-port system fails to describe the diffraction orders in air. Apparently, the influence of the diffraction orders on the phase difference at Brewster's angle is small, and the truncated scattering matrix accurately captures the physical process related to the reversal of the Fano lineshape.

To emphasize that in the asymmetric case the direct reflectivity does not reach zero while the asymmetry of the Fano lineshape is reversed, Figure 5.6 shows the calculated reflection spectra (solid lines), for angles of incidence from 72° to 80° in steps of 2°. The spectra are offset vertically by 0.2 for clarity, with the horizontal dash-dot lines indicating zero reflectance. It is clear from the figure that the asymmetry reversal occurs between 76° and 78°, but that the direct reflectivity does not reach zero for the entire angle range from 72° to 80°.

The corresponding phase difference $\Delta\xi$ between the direct and the resonant contribution is shown by the solid line in Fig. 5.7. The parameters of the structure are identical to those of the symmetric structure of Fig. 5.5, with the only difference that the air on one side has been replaced by a dielectric with a refractive index of 1.4. As can be seen, the phase difference goes through zero for an angle of incidence of 77.2°, which is larger than Brewster's angle for the symmetric structure. Similar to the symmetric structure we observe abrupt changes in the phase difference due to higher order diffraction in the

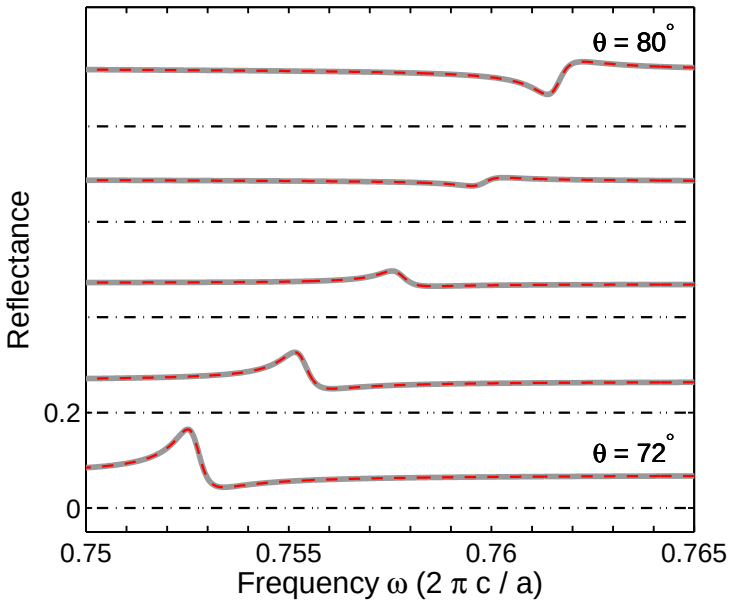

Figure 5.6. Calculated reflection spectra for an asymmetric structure (solid lines), for angles of incidence from 72° to 80° in steps of 2°, vertically offset by 0.2 for clarity, showing the asymmetry reversal of the *p*-polarized (-1,±1) mode. Note that the zero in the amplitude reflection coefficient is indicated by the dash-dot lines, for each reflectivity spectrum. Dashed lines show the fit of the Fano model to the calculated data.

air and in the substrate, as indicated by the vertical arrows. The inset shows the dispersion relation of the leaky mode (solid line) together with folded light lines in air (dashed line) and in the substrate (dash-dot lines). From the crossings of these lines with the dispersion of the leaky mode we conclude that there are four higher diffraction orders. The diffraction order into the substrate that uses the (-1,0) reciprocal lattice vector is present for all angles of incidence.

The dashed line in Figure 5.7 shows the calculated phase difference using coupled-mode theory of Section 5.4.2 truncated to only two modes. In the calculation we use the same effective refractive index for the slab as a function of frequency (Eq. 5.9) as obtained for the symmetric slab, since the increase in the effective refractive index caused by the gel substrate is small. As can be seen, the truncated coupled-mode theory reproduces the main features in the phase difference. We note a slight difference in the angle where the Fano

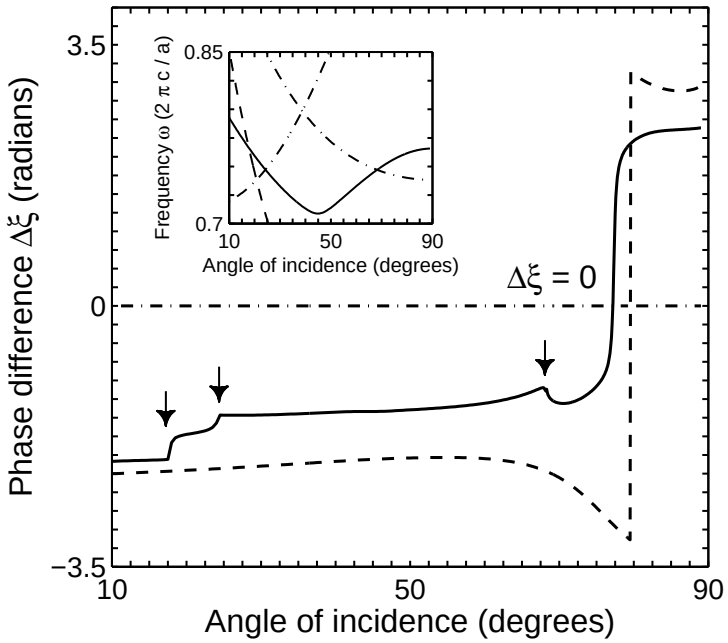

Figure 5.7. Calculated phase difference between the resonant and the non-resonant contribution, as a function of the angle of incidence, for an asymmetric structure (solid line). The phase difference is obtained for the *p*-polarized (-1,±1) mode at the resonance frequency, by fitting a Fano model to the calculated reflection spectra. The asymmetry reversal of the Fano lineshape ($\Delta\xi = 0$) occurs beyond Brewster's angle for the symmetric structure. The dashed line represents the phase difference calculated using a coupled-mode theory with only two modes, as described in the text. The inset shows the calculated dispersion relation of the leaky mode (solid line), and the folded light lines in both air (dashed line) and gel (dash-dot lines).

lineshape reversal occurs between the truncated model and the full calculation. This difference can be attributed to the presence of higher order diffraction. For a lossless system, the amplitude of the resonance should be equal to 1, when there is no higher order diffraction. Due to the higher order diffraction, the amplitude of the resonance in Fig. 5.6 is significantly reduced. Nevertheless, we believe that the truncated model accurately describes the physical process underlying the reversal of the Fano lineshape.

5.5 Conclusions

The measured reflectivity spectra for p-polarized light for a photonic crystal slab on a gel substrate, show several Fano lineshapes on top of a slowly varying background. The asymmetry of the Fano lineshape can be reversed by tuning the angle of incidence. For symmetric slabs, with air on both sides, the angle at which the asymmetry reverses is equal to Brewster's angle, and the direct contribution reaches zero. For asymmetric slabs this is no longer true: the reversal is observed for an angle of incidence beyond Brewster's angle, and the direct reflectivity no longer reaches zero. A truncated two-port coupled-mode theory can be applied to both the symmetric and the asymmetric structures, which reveals the underlying mechanism of the asymmetry reversal. For asymmetric photonic crystal slabs with $d/a < 0.5$, the reversal of the asymmetry occurs for angles larger then Brewster's angle. We show that the resonances in reflection spectra of a lossless photonic crystal waveguide should be described by a complex q parameter in the Fano model. Only for a symmetric structure the q parameter, which gives the ratio between the resonant and the direct contribution, can be taken as real. The reversal of the asymmetry occurs whenever the phase difference between the resonant and the non-resonant contribution is an integer multiple of π, which does not necessarily coincide with a minimum in the direct reflectivity.